Chapter 7

One-Photon Absorption-Based Direct Laser Writing of Three-Dimensional Photonic Crystals

Dam Thuy Trang Nguyen, Mai Trang Do, Qinggle Li, Quang Cong Tong, Thi Huong Au and Ngoc Diep Lai

Additional information is available at the end of the chapter

http://dx.doi.org/10.5772/intechopen.71318

Abstract

A simple and low-cost technique called low one-photon absorption (LOPA) direct laser writing (DLW) is demonstrated as an efficient method for structuration of multidimensional submicrostructures. Starting from the diffraction theory of the electromagnetic field distribution of a tightly focused beam, the crucial conditions for LOPA-based DLW are theoretically investigated, and then experimentally demonstrated using a simple optical confocal microscope. Various 1D, 2D, and 3D submicrostructures were successfully fabricated in different materials, such as commercial SU8 photoresist and magnetic nanocomposite. The advantages and drawbacks of this LOPA-based DLW technique were also studied and compared with the conventional two-photon absorption based DLW. Several methods were proposed to overcome the existing problem of the DLW, such as the dose accumulation and shrinkage effect, resulting in uniform structures with a small lattice constant. The LOPA-based DLW technique should be useful for the fabrication of functionalized structures, such as magneto-photonic and plasmon photonic crystals and devices, which could be interesting for numerous applications.

Keywords: direct laser writing, one-photon absorption, photonic crystal, magnetic nanocomposite, magneto-photonic microstructures

1. Introduction

In recent years, various fabrication techniques have been proposed and implemented to realize structures at micro- and nanoscales, opening numerous applications such as micro-machining, optical data storage, nanophotonics, plasmonics, and bio-imaging, etc. [1–4]. Among those techniques, optical lithography, which includes mask lithography [5, 6], interference

or holography photolithography [7–9], and direct laser writing [10–13], is the most popular because of its simplicity, flexibility and capability of producing different kinds of microstructures, addressing a variety of applications.

The fundamental working principle of the optical lithography involves the use of a photoresist, a light-sensitive material, which changes its chemical property when exposed to light. Based on the reactions of photoresists to light, they are classified into two types: positive photoresist and negative photoresist. With positive photoresists, the areas exposed to the light absorb one or more photons and become more soluble in the photoresist developer. These exposed areas are then washed away with the photoresist developer solvent, leaving the unexposed material. With negative resists, exposure to light causes the polymerization of the photoresist chemical structure, which is just the opposite of positive photoresists. The unexposed portion of the photoresist is then dissolved by the photoresist developer. Light sources of different wavelengths are used based on the purposes of the fabrication, which involve the absorption mechanisms of the used photoresist. There are two types of absorption mechanisms, namely one-photon absorption (OPA) and two-photon absorption (TPA). The OPA excitation method is an ideal way to fabricate one- and two-dimensional (1D and 2D) thin structures [14]. In this technique, a simple and low-cost continuous-wave (CW) laser operating at a wavelength located within the absorption band of the thin film material is used as the excitation source. Wavelengths in the UV range or shorter are commonly used to achieve high resolution [15]. This method is usually applied in mask lithography and interference techniques, where an entire pattern over a wide area is created in seconds. All structures are often realized at the same time; therefore, these techniques are called parallel processes. However, due to the strong absorption effect, light is dramatically attenuated from the input surface. Thus, it is impossible for OPA to address thick film materials or 3D optical structuring.

The TPA (or multi-photon absorption) technique presents a better axial resolution. In this case, two low energy photons are simultaneously absorbed inducing the optical transition from the ground state to the excited state of the material, equivalent to the case of linear absorption (OPA). Two-photon absorption is a nonlinear process, which is several orders of magnitude weaker than linear absorption, thus very high light intensities are required to increase the number of such rare events. In practice, the process can be achieved using a pulsed (picosecond or femtosecond) laser. The TPA method is commonly applied for the technique called direct laser writing (DLW), in which a pulsed laser beam is focused into a sub-micrometer spot, resulting in a dramatic increase of the laser intensity at the focusing spot. Hence, TPA-based 3D imaging or fabrication can be achievable [4, 11, 12] with high spatial resolution.

Indeed, DLW has been proved to be an ideal way to fabricate sub-micrometric arbitrary structures, offering flexibility, ease of use, and cost effectiveness. As opposed to mask lithography and interference techniques, DLW is a serial process in which a structure is realized by scanning the focusing spot following a desired pattern. Thus, any arbitrary 1D, 2D, and 3D periodic or non-periodic pattern can be fabricated on demand.

However, as mentioned above, the TPA-based DLW requires the use of a femtosecond or picosecond laser and a complicated optical system, making it a rather expensive fabrication technique. Recently, an original method called LOPA (low one-photon absorption) DLW has

been demonstrated [16, 17], allowing one to combine the advantages of both OPA and TPA methods. Indeed, the LOPA method employs a simple, CW and low power laser, as in the case of conventional OPA, but it allows the optical addressing of 3D objects, as what could be realized by the TPA method, by using a combination of an ultralow absorption effect and a tightly focusing spot. The illustration of an absorption spectrum of photoresist shown in **Figure 1(a)** represents three absorption mechanisms, which are shown in **Figure 1(b)**: conventional OPA (solid ring), LOPA (dashed ring) and TPA (dash-dotted ring), respectively. If a laser beam, whose wavelength is positioned at the edge of the absorption band where the absorption is ultralow, is applied, the light intensity distribution remains almost the same as in the absence of material. In short, by tightly focusing an optical beam inside a thick material with a very low absorption at the operating wavelength, it is possible to address 3D imaging and 3D fabrication, as what realized by TPA method. As compared to the latter one, this LOPA-based DLW is very simple and inexpensive and it allows one to achieve very similar results.

This chapter presents theoretically and experimentally this original fabrication method, LOPA-based DLW technique, which allows the realization of multidimensional sub-micrometer photonic crystals. The advantages of this fabrication method will also be presented and compared with other fabrication techniques.

In Section 2, the theory of the LOPA-based DLW method and experimental conditions to realize 3D sub-microstructures are presented. In this case, the vectorial diffraction theory of a laser beam, tightly focused by a high numerical aperture objective lens, is extended taking into account the very low absorption of the propagating medium. Numerical calculations will also be shown.

In Section 3, it will be demonstrated experimentally that any sub-micrometer 1D, 2D, and 3D structures can be realized by the LOPA-based DLW technique, by choosing appropriate photoresist and excitation laser wavelength.

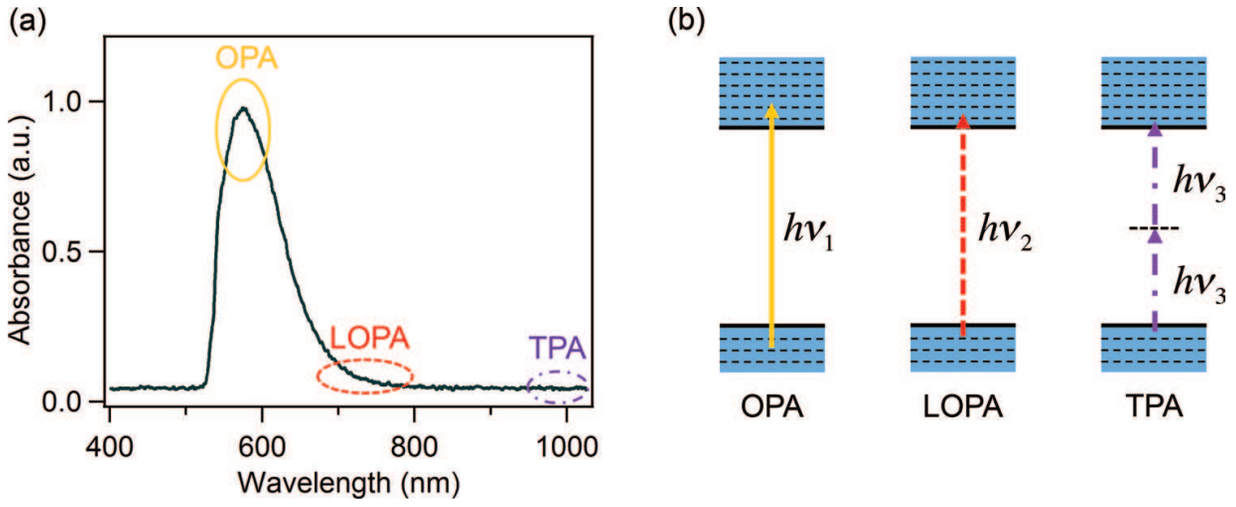

Figure 1. (a) Illustration of the absorption spectrum of a photoresist. The three rings illustrate three ranges of wavelength corresponding to (b) three absorption mechanisms: standard one-photon absorption (OPA), low one-photon absorption (LOPA), and two-photon absorption (TPA).

In Section 4, different additional methods to optimize the LOPA-based DLW are demonstrated in order to obtain sub-microstructures, which show high uniformity, less shrinkage, and with a lattice constant smaller than the diffraction limit.

To demonstrate the versatility of the LOPA-based DLW, in Section 5, the fabrication of magneto-photonic sub-microstructures for biomedical engineering realized by the LOPA-based DLW technique is presented. This opens many promising applications, such as tunable photonic structures based on magneto-optical effect and development of microrobotic tools for transport in biological systems.

In the last section, some conclusions of the newly developed LOPA-based DLW technique, advantages this technology brings to the photonic crystal field, as well as some prospects will be discussed.

2. Theory of LOPA-based DLW technique

In this section, the vectorial Debye approximation is presented, based on which a new mathematics representation is further established, where the absorption effect of the material is taken into account when a light beam propagates through an absorbing medium. Based on the new evaluation form of vectorial Debye theory, the influence of absorption coefficient of the studied material, the numerical aperture (NA) of the objective lens (OL), and the penetration depth of light beam on the formation of a tight focusing spot are investigated. From that, the crucial conditions for the realization of LOPA microscope and LOPA DLW are established.

2.1. Electromagnetic field distribution of a tight focused beam in an absorbing medium

The mathematical representation of the electromagnetic field distribution in the focal region of an OL was proposed by Wolf in the 1950s [18]. This theory based on the vectorial Debye approximation allows the calculation and prediction of the intensity and polarization distributions of a light beam focused inside a material by a high NA OL. Nonetheless, the influence of material absorption on the intensity distribution and the focused beam shape of a propagating optical wave have not been systematically investigated yet. In this section, the mathematical representation proposed by Wolf [18] will be employed, taking into account the absorption effect of the material when a focused light beam propagates through it, in order to investigate the intensity distribution, especially in the focal region.

The schematic representation of light focusing in an absorption medium is shown in **Figure 2**. D is the interface between the transparent material, such as a glass substrate or air, and the absorbing material. To simplify the problem, it is assumed that the refractive index mismatch problem arising at any interface is negligible. d represents the distance between the D interface and the focal plane. The electromagnetic field near the focal plane in Cartesian coordinates (x, y, z) [16, 19] is represented by,

$$\mathbf{E} = -\frac{ikC}{2\pi} \iint_{\Omega} \mathbf{T}(s) A(s)\, e^{[ik(s_x x + s_y y + s_z z)]}\, ds_x\, ds_y, \tag{1}$$

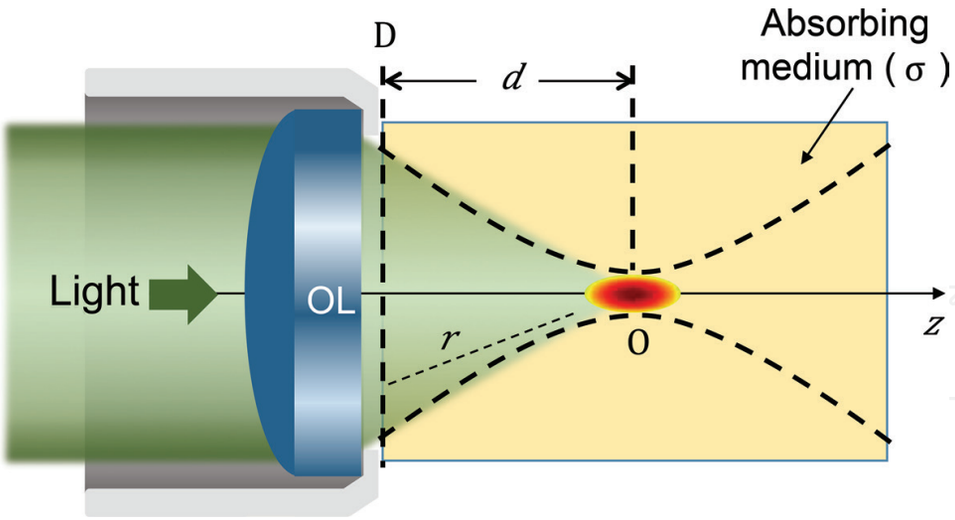

Figure 2. Schematic representation of a tightly focused light beam inside an absorbing medium. σ is the absorption coefficient of the medium, O is the focal point, D is the interface between the transparent and the absorbing media, r is the distance from an arbitrary point on the D plane to the focal point, and d is the distance between the D plane and the focal plane of the objective lens.

where C is a constant, k is the wave number ($k = 2\pi n/\lambda$), n is the refractive index of the absorbing medium, λ is the excitation wavelength, Ω is a solid angle corresponding to the objective aperture, $\mathbf{S} = (s_x, s_y, s_z)$ is the vector of an arbitrary optical ray, and $\mathbf{T}(s) = \mathbf{P}(s)\mathbf{B}(s)$is a transmission function where $\mathbf{P}(s)$ is the polarization distribution and $\mathbf{B}(s)$ is the amplitude distribution at the exit pupil. $A(s)$ represents the absorption effect of the material, which is expressed as $A(s) = \exp(-\sigma r)$, where σ is the absorption coefficient and r indicates the optical path of each diffracted light ray in the absorbing medium, which is defined as the distance from a random point located in the D plane to the focal point, as shown in **Figure 2**. For calculations, r is determined by

$$r = \sqrt{(x'-x)^2 + (y'-y)^2 + (d-z)^2}, \tag{2}$$

where (x', y', d) gives the position of an arbitrary diffracted light ray located on the D plane. Theoretically, Eq. (1) allows calculation of the light distribution resulting from the interference of all light rays diffracted by the exit pupil of the OL. However, in practice, the light intensity and the focus shape at the focus region depend strongly on the absorption term $A(s)$ since light is absorbed by the material in which it propagates and its amplitude decreases along the propagation direction.

The light intensity distribution, also called point spread function (PSF), in the focal region of the OL is defined as

$$I_{PSF} = \mathbf{E}\mathbf{E}^* \tag{3}$$

This theory is applicable for any cases, OPA, LOPA, or TPA. It can be seen that the EM field distribution in the focal region depends on various parameters, such as the polarization of

incident light, the NA of OL, the absorption coefficient of the material, etc. It is impossible to have an analytical solution of the light field at the focusing spot of a high NA OL. However, it can be numerically calculated, which will be shown in the next part.

2.2. Numerical calculation of point spread function

In order to numerically calculate the light intensity distribution, the I_{PSF} equation was programmed by a personal code script based on Matlab software, with the influence of different input parameters including the absorption coefficient of the studied material, the NA of the OL, and the penetration depth of the light beam.

First, the influence of the absorption effect of the SU8 material, which will be used later for experimental demonstration in the next sections, was investigated. Based on the absorption spectrum of SU8 shown in **Figure 5(b)**, three typical wavelengths to calculate the intensity distribution in the focal region were chosen, representing three cases of interest: conventional OPA (308 nm), LOPA (532 nm) and TPA (800 nm), respectively. The corresponding absorption coefficients in each case are: $\sigma_1 = 240{,}720\ m^{-1}$ ($\lambda_1 = 308$ nm), $\sigma_2 = 723\ m^{-1}$ ($\lambda_2 = 532$ nm), and $\sigma_3 = 0\ m^{-1}$ ($\lambda_3 = 800$ nm). The absorption interface (D) was arbitrarily assumed to be separated from the focal point O by a distance of 25 μm, the NA of the OL was chosen to be 0.6, the refractive index (n) of SU8 is 1.58. As seen in **Figure 3(a_1)**, the incoming light is totally attenuated at the interface D because of the strong absorption of SU8 at 308 nm, which explains why it is not possible to optically address 3D object with the conventional OPA method. However, when using an excitation light source emitting at 800 nm, the absorption coefficient is zero, thus light can penetrate deeply inside the material, resulting in a highly resolved 3D intensity distribution. The numerical calculation result derived from the quadratic dependence of the EM field is shown in **Figure 3(a_3)**. The size of the focusing spot (full width at half maximum, FWHM) is quite large due to the use of a long wavelength. However, in practice, two photons can only be simultaneously absorbed at an intensity above the polymerization threshold. Therefore, a small effective focusing spot below the diffraction limit can be achieved with the TPA method by controlling the excitation intensity.

The case where the linear absorption is very low (LOPA) was considered. At the wavelength $\lambda = 532$ nm, the absorption coefficient is only $723\ m^{-1}$, which is much smaller than that at 308 nm. Simulation results show that light can penetrate deeply inside the absorbing material without significant attenuation thanks to this very low linear absorption. As shown in **Figure 3(a_2)**, the light beam can be tightly confined at the focusing spot, which can then be moved freely inside the thick material, exactly as in the case of TPA. Furthermore, LOPA requires a shorter wavelength as compared with TPA, the focusing spot size (FWHM) is therefore smaller. The diagram depicted in **Figure 3(a_4)** shows clearly the difference of the intensity distribution along the optical axis of three excitation mechanisms. It is important to note that there is no intensity threshold in the case of LOPA, because it is a linear absorption process. Therefore, LOPA requires a precise control of light dose in order to achieve high resolution optical addressing.

The NA of OL is also an important parameter to be taken into account for LOPA case. It was demonstrated that the use of a high NA OL is a crucial condition. The intensity distributions at the focusing spot obtained with OLs of different NA values (with the same low absorption

http://dx.doi.org/10.5772/intechopen.71318

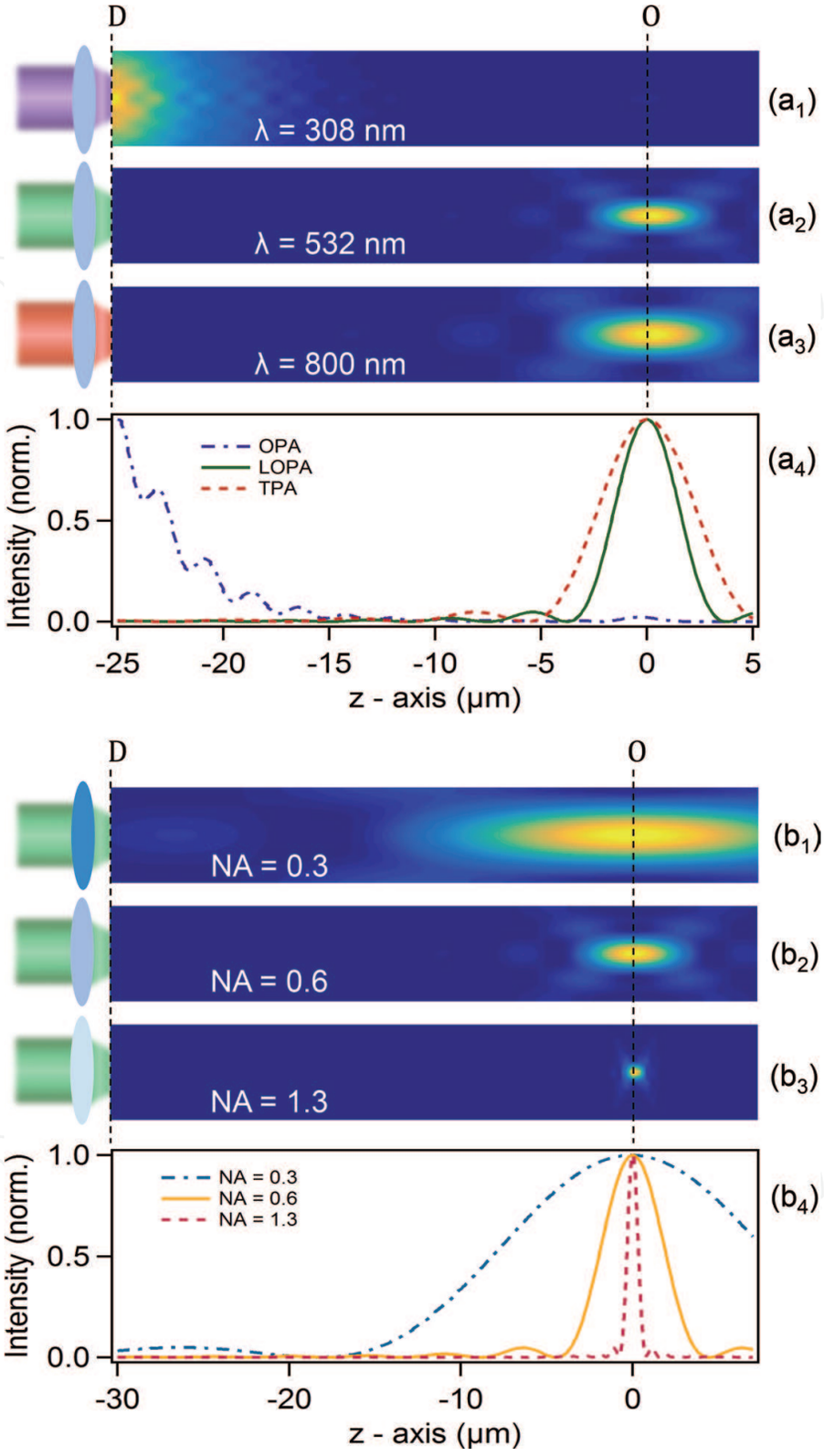

Figure 3. (a) Numerical calculations of light propagation inside SU8, by using different wavelengths, (a_1) 308 nm, (a_2) 532 nm, and (a_3) 800 nm, respectively. (a_4) Intensity distributions along z-axis of the light beams shown in ($a_{1–3}$). In this calculation, NA = 0.6, refractive index n = 1.58, and d = 25 μm. (b) Propagation of light (λ = 532 nm) inside SU8, with (b_1) NA = 0.3, (b_2) NA = 0.6, and (b_3) NA = 1.3, respectively, d = 30 μm. (b_4) Intensity distributions along z-axis of the light beams shown in ($b_{1–3}$).

coefficient $\sigma_2 = 723\ m^{-1}$) are shown in **Figure 3(b)**. It is clearly seen that with an OL of low NA (NA = 0.3), the light beam is not well focused, resulting in low contrast intensity distribution between the focal region and its surrounding. Therefore, the LOPA-based microscopy using a low NA OL cannot be applied for 3D optical addressing. However, in the case of tight focusing (for example, NA = 1.3), the light intensity at the focusing spot is a million time larger than that at out of focus, resulting in a highly resolved focusing spot (**Figure 3(b_3)**).

For all the above calculations, it can be concluded that the LOPA-based microscopy is promising for the realization of 3D imaging and 3D fabrication, similarly to what could be realized by TPA microscopy. By using the LOPA technique, 3D fluorescence imaging or fabrication of 3D structures can be realized by moving the focusing spot inside the material since fluorescence (for imaging) or photopolymerization (for fabrication) effects can be achieved efficiently within the focal spot volume only.

It is worth noting that in LOPA technique, the absorption exists, even if the probability is very small, the penetration depth is therefore limited to a certain level. This effect exists also in the case of TPA, but it is more important for LOPA. **Figure 4** represents the maximum intensity at the focusing spot as a function of the penetration length, d. For this calculation, the ultralow absorption coefficient of SU8 at $\lambda = 532$ nm, $\sigma = 723\ m^{-1}$ was considered. At the distance of 390 μm, the intensity was found to decrease by half with respect to that obtained at the input of absorbing material (D interface). This penetration depth of several hundred micrometers is fully compatible with the scanning range of piezoelectric stage (typically, 100 μm for a high resolution), or with the working distance of microscope OL (about 200 μm for a conventional high NA OL).

In summary, in order to realize the LOPA-based microscopy, two important conditions are required: (i) ultralow absorption of the studied material at the chosen excitation wavelength, and (ii) a high NA OL for tight focusing of the excitation light beam. To experimentally demonstrate the application of LOPA in DLW, in the next chapter, SU8 will be used as the material and a CW laser at $\lambda = 532$ nm as the excitation source.

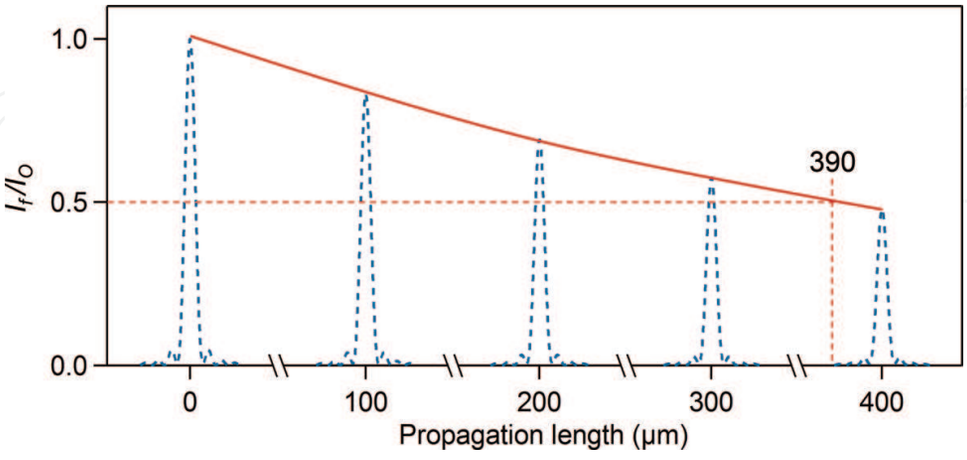

Figure 4. Red curve: normalization of intensity (I_f/I_0) at the focusing spot as a function of the propagation length. I_f and I_0 are the intensities obtained with and without absorption medium, respectively. Dot curves: zoom on intensity profiles of the focusing spot along the optical axis, calculated at different d. The results are simulated with: $\sigma = 723\ m^{-1}$; $\lambda = 532$ nm; NA = 1.3 ($n = 1.58$).

http://dx.doi.org/10.5772/intechopen.71318

3. Experimental demonstration of LOPA-based 3D microfabrication

3.1. Experimental setup and fabrication procedure

The LOPA technique can obviously be used for all 3D applications, including 3D imaging and 3D fabrication. As mentioned in section 2, two conditions are required: a photoresist that presents an ultralow absorption at the wavelength of the excitation laser, and a high focusing confocal laser scanning (CLSM) system. For the first condition, SU8 photoresist is an excellent candidate, thanks to its ultralow absorption in the visible range, for example at 532 nm (**Figure 5(b)**), which is the wavelength of a very popular and low-cost laser. By using a high NA oil-immersion OL of NA = 1.3 to focus a laser beam into the photoresist, the second condition is then satisfied.

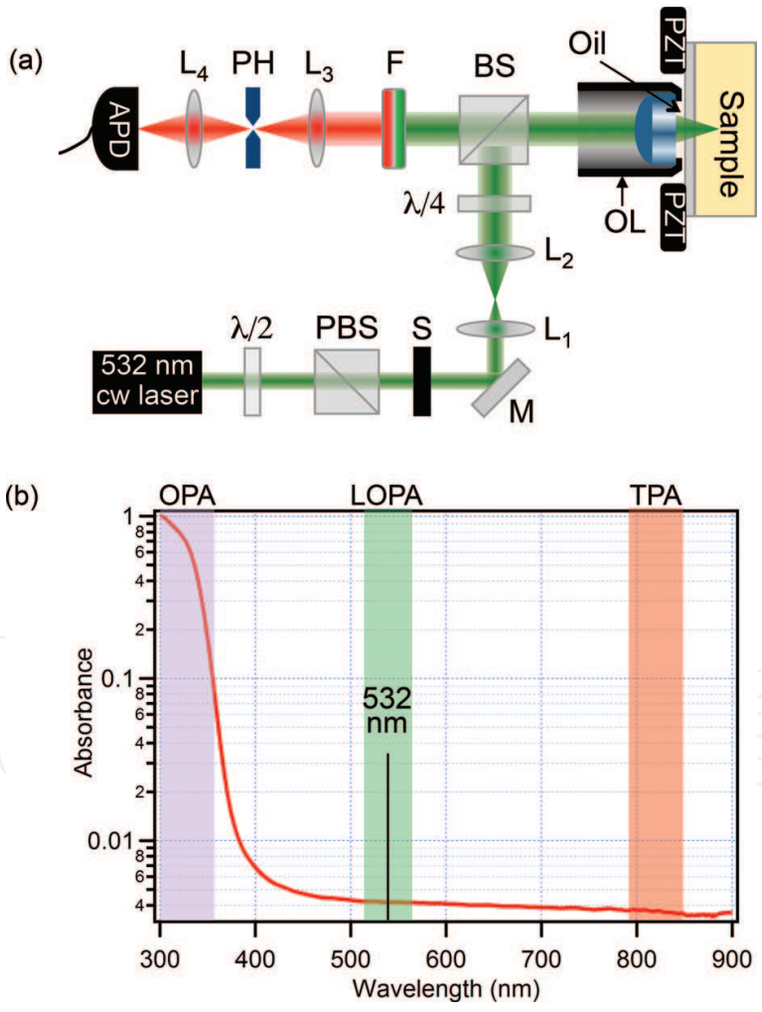

Figure 5. (a) A sketch of the experimental setup. PZT: piezoelectric translator, OL: oil immersion microscope objective, $\lambda/4$: quarter-wave plate, $\lambda/2$: half-wave plate, BS: beam splitter, PBS: polarizer beam splitter, M: mirror, S: electronic shutter, L_{1-4}: lenses, PH: pinhole, F: 580 nm long-pass filter, APD: avalanche photodiode. (b) Absorption spectrum of SU8 photoresist. The color bars indicate three cases: OPA (purple bar), LOPA (green bar), and TPA (red bar). To demonstrate LOPA DLW, a laser operating at 532 nm is used.

In order to demonstrate the LOPA DLW technique, a confocal optical system illustrated in **Figure 5(a)** was built. In this system, a CW laser operating at 532 nm is used. The laser power is monitored by a combination of a half-wave plate ($\lambda/2$) and a polarizer. The laser beam is directed and collimated by a set of lenses and mirrors. In order to realize mapping or fabrication, samples are mounted on a 3D piezoelectric actuator stage (PZT), which is controlled by a LabVIEW program. A quarter-wave plate ($\lambda/4$) placed in front of the OL is inserted and oriented to generate a circularly polarized beam for mapping and fabrication. The high NA oil-immersion objective (NA = 1.3) placed beneath the glass coverslip is used to focus the excitation laser beam. The fluorescence signal emitted by the samples is collected by the same objective, filtered by a 580 nm long-pass filter, and detected by an avalanche photodiode (APD).

For fabrication, SU8 photoresist is coated on a glass substrate. In order to remove all contamination on the surface, glass substrates must be treated with acetone and an ultra-sonication prior to the spin coating. After the cleaning process, SU8 of different viscosities (SU8 2000.5, SU8 2005, or SU8 2025) is spin coated on the glass substrates, depending on the types of the desired structure. For 1D and 2D structures, SU8 2000.5 and 2002, which give a layer thickness of 0.5 and 2 μm, are used. For 3D structures, other types of SU8 at higher viscosity, for example SU8 2005 or 2025, are required. The spin coating step is followed by a soft baking step at 65°C and 95°C, the soft baking time depends on the types of SU8 used.

Before writing the structure on the photoresist, the interface between the glass substrate and the photoresist layer must be determined. To determine the interface, the focusing spot is scanned along *xz* or *yz* plane at very low laser power to prevent polymerization, and the fluorescence signal can be collected by the APD. This step allows one to precisely write the structure at the desired position. Then the laser power is increased to several mW to fabricate any desired structures by scanning the focusing spot along a path programmed with Labview. Post exposure bake (PEB) is carried out after the fabrication, and followed by a development step.

3.2. Verification of LOPA-based fabrication

It has been demonstrated, by analyzing fluorescence emission, that the SU8 photoresist linearly absorbs the excitation laser at 532 nm-wavelength [17]. For the LOPA CLSM, the intensity at the focusing region (of the order of 10^7 W/cm^2) is much higher than that at the input of the optical system (10^{-2} W/cm^2), allowing the excitation and fluorescence detection of the focal spot volume only. The fluorescence measurements in which the emission is quite low are enabled by the use of an avalanche photodiode (APD).

By using the standard fabrication process described in the previous part, it was demonstrated that polymerization is achieved only at the focusing spot of the microscope objective, where the excitation intensity is sufficiently high to compensate the low linear absorption of the resist. In the case of TPA, there are two thresholds: the first one related to light intensity, above which two photons are simultaneously absorbed, and the second one related to dose, above which complete photopolymerization is achieved. However, in the case of LOPA, there exists only one threshold related to dose. Thanks to a high intensity at the focusing spot, the complete photopolymerization is only achieved in this region. **Figure 6** shows SEM images of experimental results. For each exposure, a solid structure, called "voxel," corresponding to

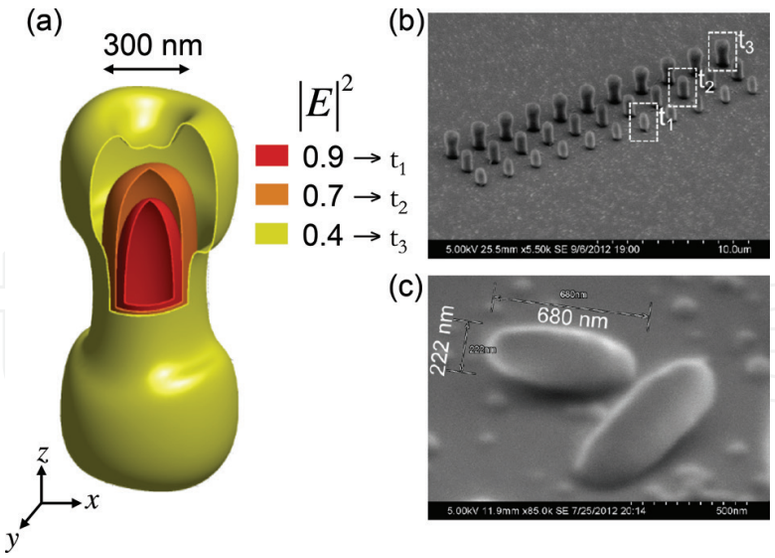

Figure 6. Fabrication of voxels by single-shot exposure. (a) Theoretical calculation of the contour plot of light intensity at the focusing region (NA = 1.3, n = 1.518, λ = 532 nm). (b) SEM image of a voxels array obtained by different exposure doses. Three ranges of voxels are fabricated correspondingly to the exposure time t_1, t_2 and t_3 whose corresponding doses are 0.9, 0.7 and 0.4 as indicated in (a). These experimental results explain the OPA nature where the formed voxel shape is determined by the exposure dose. (c) Complete voxel lying on the substrate indicated an ellipsoidal form (exposure time t_1 was applied). This form is similar to that obtained by the TPA method.

a focusing spot, was obtained. By changing either the excitation power or the exposure time, i.e. the dose, the voxel size and shape can be adjusted, as shown in **Figure 6(b)**. A CW green laser power of only 2.5 mW and an exposure time of about 1 second per voxel were required to create these structures. **Figure 6(b)** shows, for example, a voxel array realized with three different exposure times. The dose dependence can be explained theoretically by calculating the iso-intensity of the focusing spot at different levels. Three kinds of voxels obtained with t_1, t_2 and t_3 in **Figure 6(b)** correspond to three different iso-intensities illustrated in **Figure 6(a)**, namely 0.9, 0.7 and 0.4, respectively. The operation in the OPA regime is fully confirmed by the evolution of voxel size and shape observed experimentally. Indeed, in the case of TPA, the creation of bone-like voxel shape requires very high excitation intensity and could not be easily realized due to the TPA intensity threshold. In the case of LOPA, all these voxels shapes were obtained by simply adjusting the exposure time while the laser power is kept at a low value. Smaller voxels as shown in **Figure 6(c)** require shorter exposure times. Certainly, the exposure time required to create sub-micrometer structures varies as a function of the laser power.

Pillar arrays were also fabricated by scanning the focusing spot of the laser along the thickness of a 1 μm SU8 film with different writing speeds. **Figure 7** shows the pillar size as a function of writing velocity for three values of laser power, P = 7.5, 6, and 4.5 mW. The fabrication of smaller pillars down to 190 nm is possible [17]. The size of individual pillars is quite small when considering the wavelength (532 nm) used for the writing process. As for the linear dependence with intensity (OPA vs. TPA) [20, 21], the diameter-dose relationship agreement confirms this behavior, as the intensity I_0 is used for the fit, instead of I_0^2 in the case of TPA. This result confirms the fabrication of sub-microstructures by LOPA-based DLW method.

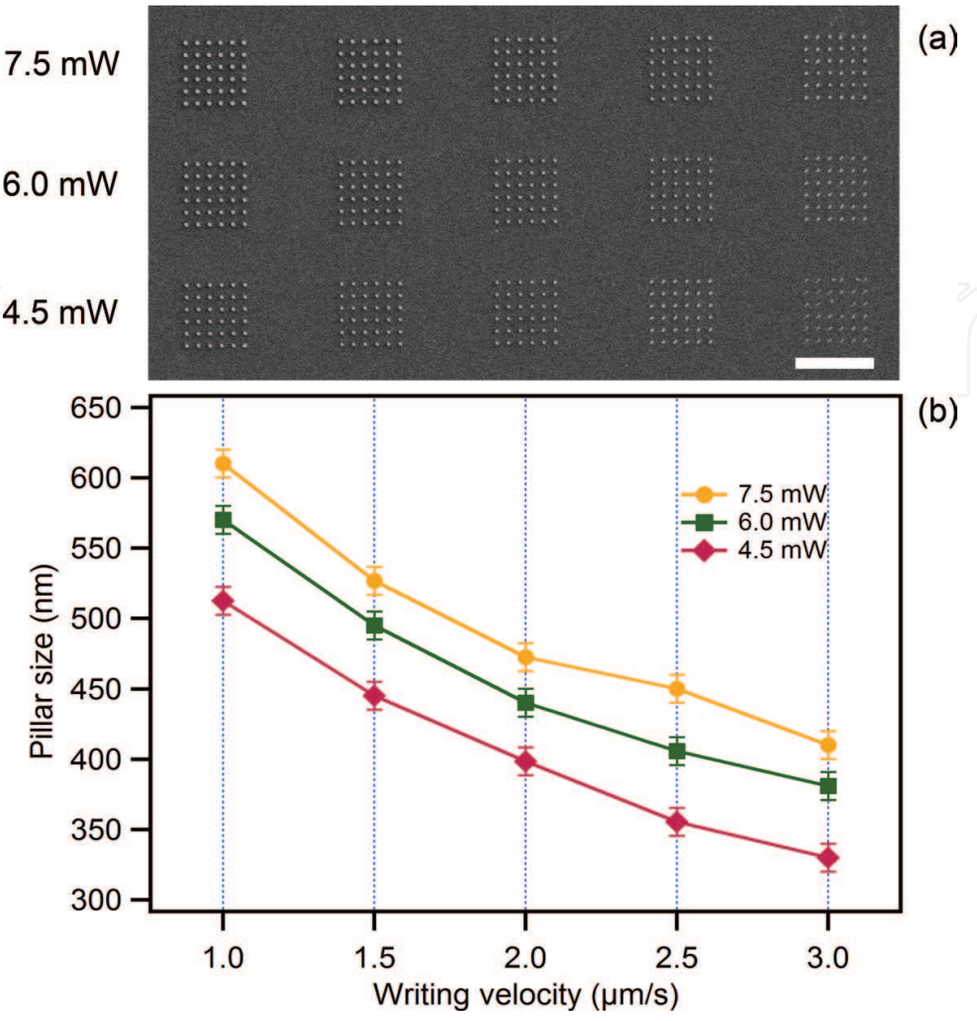

Figure 7. (a) SEM image of a pillar arrays fabricated at different writing velocity and laser powers. (b) Dose dependence of size of pillars shown in (a), with different laser power values, $P = 7.5$, 6, 4.5 mW, and different writing velocities, $v = 1.0$, 1.5, 2.0, 2.5, and 3.0 μm/s. Scale bar: 10 μm.

3.3. LOPA-based DLW for 3D microstructure fabrication

In order to demonstrate 3D fabrication, 3D arbitrary photonic crystals (PCs) have been realized. In the fabrication process, the dose was adjusted by changing the velocity of the PZT movement while the input power is fixed. The doses were varied from structure to structure depending on the size and separation (periodicity of PC). In the first experiment, a series of different size 3D woodpile PC structure on glass substrate was fabricated. It is noted that, SU-8 exhibits a strong shrinkage effect, which results in the distortion of the fabricated structure. After a number of experiments, acceptable parameters for woodpile, which are an input power of 2.5 mW and a velocity of 1.4 μm/s, were found. Applying these parameters, 3D diamond lattice-like-based PC structures such as woodpile, twisted chiral and circular spiral can be realized.

Figure 8(a–f) shows SEM images of 3D woodpile, spiral and chiral PCs fabricated with these optimum fabrication parameters. The woodpile structure (**Figure 8(a** and **b)**) consists

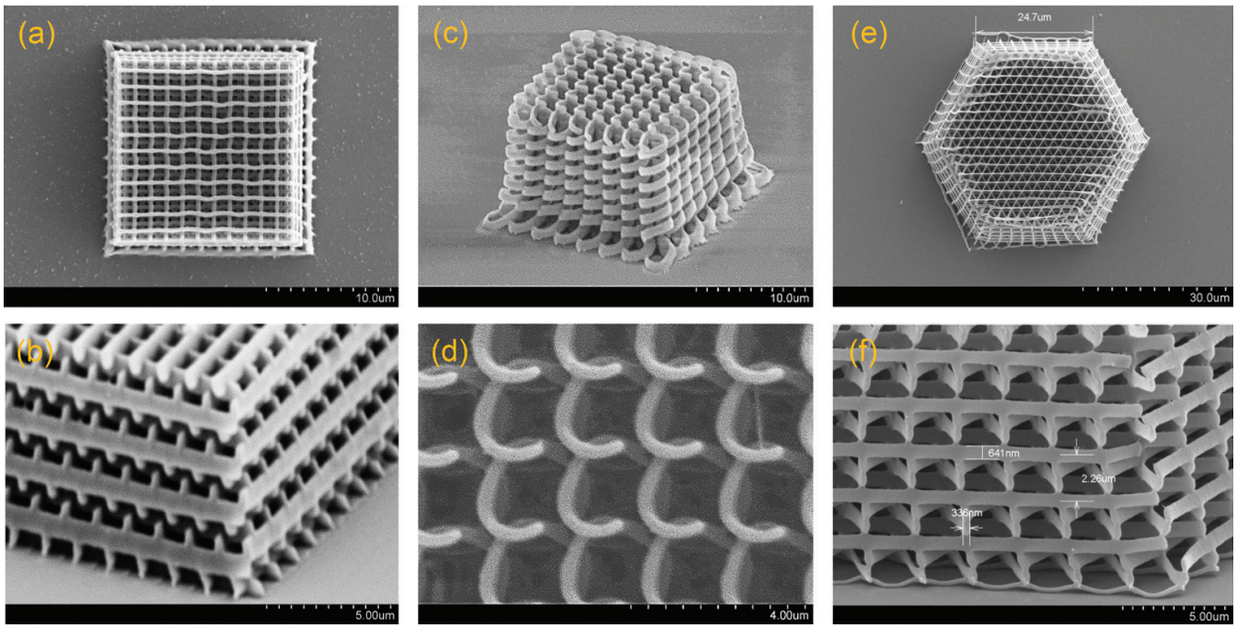

Figure 8. (a–b) SEM images of a woodpile structure fabricated with the following parameters: distance between rods = 1.5 μm; distance between layers = 0.7 μm; number of layers = 20; laser power P = 2.5 mW and scanning speed v = 1.4 μm/s. (c and d) SEM images of a chiral structure. Structure and fabrication parameters: distance between rods a = 2 μm; distance between layers c/3 = 0.75 μm; number of layers = 28; line width r = 300 nm; laser power P = 2.8 mW and scanning speed v = 1.34 μm/s. (e–f) SEM images of a spiral structure (shown in inset). Fabrication parameters: diameter of a spiral D = 2 μm; spiral pitch C = 2 μm; lattice constant a = 3 μm; spiral height equals to film thickness = 15 μm; laser power P = 2.6 mW and scanning speed v = 1.34 μm/s.

of stacked 20 layers. Each layers consists of parallel rods with period a = 1.5 μm. Rods in successive layers are rotated by an angle of 90° relative to each other. Second nearest-neighbor layers are displaced by a/2 relative to each other. Four layers form a lattice constant c = 2.1 μm. SEM measurement shows that the line width of rods on the top layer is about 320 nm, which is 1.5 times of the voxel standard size. This means that the size of the rod can be minimized further. Woodpile structure with measured separation between rods on the top layer of only 800 nm and the measured line width of 180 nm was also successfully fabricated. This result shows evidently that separation of rods and layers are comparable to the wavelength of visible light. **Figure 8(c–f)** shows, as examples, two other kinds of sub-micrometer 3D structures. Clearly, 3D chiral or spiral structures are well created, which are as good as those obtained by TPA DLW. The structures features are well separated, layer by layer, in horizontal and in vertical directions. The feature sizes are about 300 nm (horizontal) and 650 nm (vertical).

Experimental realization of LOPA-DLW in fabrication of 1D, 2D and 3D photonic crystal showed evidently the advantage of LOPA idea in combining with regular DLW. With a few milliwatts of a CW laser and in a moderate time, any kind of sub-micrometer structure with or without designed defect could be fabricated. However, some fabricated structures are not uniform or distorted. The physical causes of the distortion can be attributed to two main effects: dose accumulation effect [22] and shrinkage effects [23]. In the next section, some techniques to overcome those effects will be experimentally demonstrated.

4. Optimization of LOPA-based DLW technique

4.1. Dose accumulation effect

As a consequence of linear behavior of absorption mechanism, the dose accumulation effect is the inherent nature of linear absorption material [24, 25]. In contrast to a conventional TPA method, a photoresist operated in OPA regime does not have any threshold of polymerization [26], hence the voxel size can be controlled by adjusting the exposure dose. In principle, polymerization occurs at the focusing spot with a single-shot exposure resulting in a very small voxel (smaller than the diffraction limit) [27]. However, when two voxels are built side-by-side with a distance of about several hundred nanometers, two resulting voxels are no longer separated [17]. This issue evidently originates from the dose accumulation effect in OPA process.

Similar to OPA microscopy where the microscopy image cannot resolve two small objects which localize at about several hundred nanometers from each other, the fabricated voxels in DLW also cannot be separated. Abbe's criterion states that, the minimum resolving distance of two objects is defined as $0.61\lambda/\mathrm{NA}$, where λ is the wavelength of incident light. This diffraction barrier thus imposes the minimum distance between different voxels, created by different exposures. Moreover, when multiple exposures are applied, although isolated voxel fabrication is ideally confined to the focal volumetric spot, the superposition of many out-of-focus regions of densely-spaced voxels leads to undesired and unconfined reaction. This results in the larger effective voxel size, even with a distance far from the diffraction limit. Indeed, in the case of OPA, photons could be absorbed anywhere they are, with an efficiency depending on the linear absorption cross-section of the irradiated material. The absorbed energy is gradually accumulated as a function of exposure time.

Figure 9 shows the theoretical calculations and experimental results of the dependence of the voxels size on distance. When two voxels are separated by a distance shorter that 1 μm, a clear accumulation effect is observed, resulting in a voxel of larger size. When the separation changes from 2 to 0.5 μm, the FWHM of each voxel is increased from 190 to 300 nm. Moreover, for a short separation, the voxels array is not uniform from the center to the edge part, as can be seen in case of a separation of 0.5 μm. In the parts below, two strategies to get rid of this accumulation effect are discussed.

4.1.1. Dose compensation strategy

According to the structures fabricated by LOPA DLW and the theoretical calculation, the dose accumulation effect should be compensated in order to get superior structure uniformity. The compensation technique idea is based on a balance of the exposure doses over the structure. In other words, a certain amount of the exposure dose should be reduced at the region (or a part or a division) where the dose accumulation effect strongly occurs and should be added to the region where the dose is lacking.

As demonstrated above, the accumulation effect depends on the separation distance, s. 2D micropillars array was fabricated by scanning the focusing spot along the z-axis to demonstrate

http://dx.doi.org/10.5772/intechopen.71318

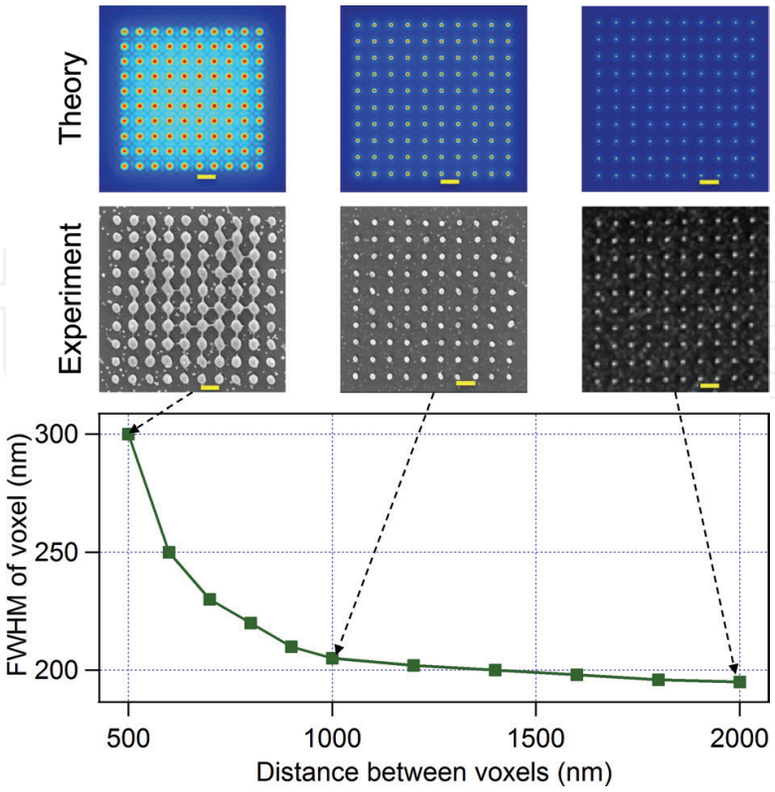

Figure 9. Dependence of voxel sizes on separation between voxels calculated at the iso-intensity = 0.5 ($I = I_0/2$), showing the influence of energy accumulation from one focusing spot to another. Insets show simulated images (blue background) and SEM images (gray background) of 2D voxel arrays fabricated with different distances between two voxels: 2, 1, and 0.5 μm. Scale bar (from left to right): 0.5, 1, and 2 μm.

the accumulation effect and the dose compensation technique. The variation of the pillars size as a function of s distance, from 0.3 to 3 μm, has been systematically investigated [22]. According to the pillars size variation, from the center to the edge of the structure, the size difference could be compensated by gradually increasing the exposure doses for outer pillars. The intensity distribution of a pillar array and the dose compensation strategy are shown in **Figure 10(a)**. Different dose compensation ratios have been experimentally applied, indicated by letters A, B, C, and D. Two sets of structures have been fabricated on the same sample in order to maintain the same experimental conditions: one without and the other with dose compensation. The accumulation effect in the case of s = 0.4 μm, obtained without compensation, is shown in **Figure 10(b)**. It can be seen that the structure is not uniform, and the outmost voxels collapse into central pillars. With dose compensation, i.e. the doses for outer pillars are increased, 2D micropillars arrays become uniform. Structures realized with different dose ratios, corresponding to A, B, C, and D schemes depicted in **Figure 10(a)**, are shown in **Figure 10(c–f)**. With high dose compensation amplitude, the size of outer pillars becomes even larger than those in the center. By using an appropriate dose compensation ratio, perfectly uniform 2D micropillars array is obtained, as shown in **Figure 10(c)**. The structure period is only 400 nm, the height of pillars is about 700 nm, and pillar's diameter is about 160 nm. Structures with periods of several hundred nanometers are very suitable for photonic applications in visible range.

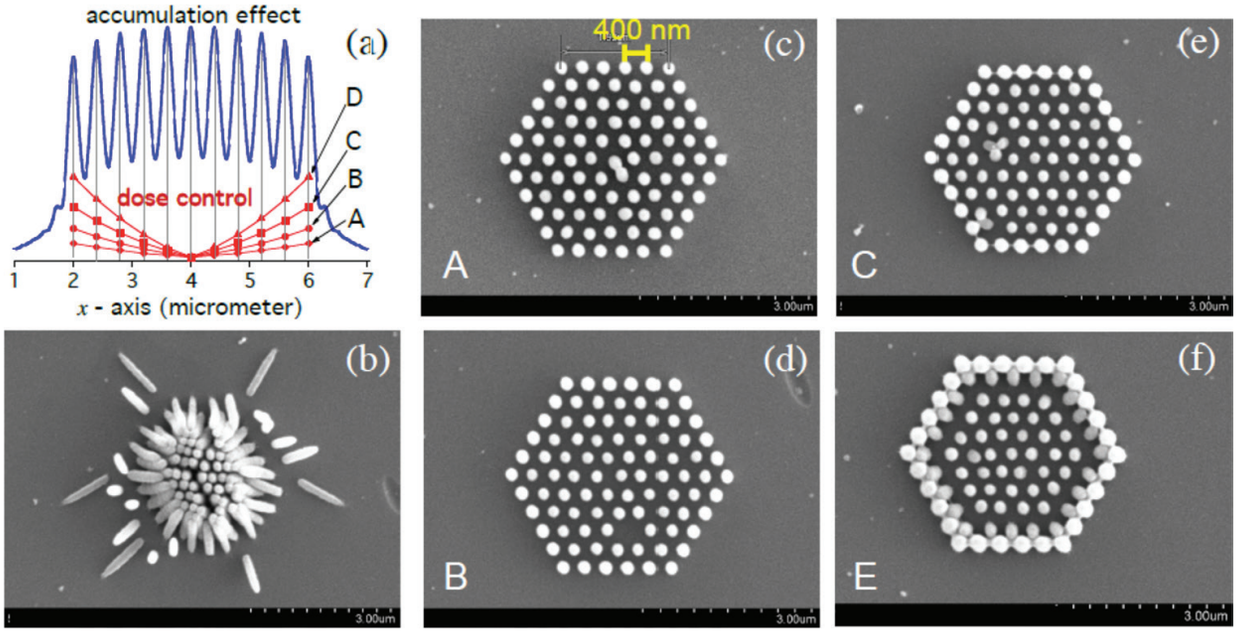

Figure 10. Compensation of dose accumulation for s = 0.4 μm. (a) Theoretical calculation of the intensity distribution as a function of x–position (blue color), and proposition of different doses, indicated by A, B, C, and D (red color) to compensate the dose accumulation effect. (b–f) SEM images of 2D hexagonal structures realized without compensation (b), and with compensation with different doses: A (c); B (d); C (e), and D (f). The excitation power was fixed at 2.5 mW and the dose was adjusted by changing the writing velocity.

4.1.2. Local PEB for small and uniform microstructures

The dose compensation technique are presented above and proved to be able to compensate the size difference in the structures. Nonetheless, this technique requires numerous calculation and tests in order to find out the appropriate dose compensation parameters. For example, for the fabrication of other 2D structures with a sub-micrometer period containing an arbitrary defect, such as a microcavity or a waveguide of arbitrary shape, the dose should be controlled for individual voxel (or pillar) as a function of its position in the structure and with respect to the defect. This requires many attempts to find out the optimized parameters since the dose compensation is different for different structures.

In this part, the thermal effect induced by a CW green laser in the LOPA-based DLW technique has been investigated, which plays a role as a heat assistant for completing the crosslinking process of the photopolymerization of SU8 [28]. The fabrication of sub-microstructures using LOPA DLW with a laser induced thermal effect, also called local PEB, was demonstrated, and it was also shown to alter the traditional PEB on a hot plate and help overcome the accumulation effect existing in standard LOPA DLW.

For the demonstration of local PEB, two sets of 2D structures were fabricated, each set contains pillar arrays written at different doses (by varying the laser power and the writing speed). One set was realized following the traditional process, i.e., after exposure, the sample was post-baked for 1 min at 65°C and then 3 min at 95°C using hot plate. For the other set, the PEB step was skipped, which means that the exposure process was followed directly by the

development process. It has been observed that for the same dose, the pillars fabricated without PEB are smaller than those fabricated with PEB [28]. Due to the fact that the structures are not formed at low power (low light intensity), it is assumed that the applied laser power or intensity must be above a threshold in order to induce enough heat for the crosslinking process, and this threshold should be higher than that of standard LOPA (with PEB) for a complete photopolymerization.

Figure 11(a) shows the accumulation effect observed in the structures fabricated using traditional PEB process at different doses. The distance between two pillars is 500 nm, which is considered as a sufficiently short separation to induce noticeable accumulation effect. It can be observed that the pillar size decreases from the center to the edge, with a variation of 10–20%, resulting in non-uniform structures. **Figure 11(b)** shows the SEM images of structures obtained using local PEB. In this case, in order to induce sufficiently high temperature, the laser power (5 mW) was higher than that (3 mW) used with traditional PEB step. In contrast to the structures fabricated using traditional PEB, which shows accumulation effect (**Figure 11(a)** on the top), the structures obtained with local PEB show nearly perfect uniformity (**Figure 11(b)** on the top). Moreover, as compared to the dose compensation method, the LOPA-based DLW using local PEB does not require testing, since the dose applied is constant for all voxels and the range of applicable doses is large. In addition, the PEB step is skipped, which is a great advantage in terms of fabrication time. Furthermore, comparing to structures realized by TPA-based DLW, the period of these fabricated structures is much shorter (only 500 nm or even 400 nm) thanks to the use of short laser wavelength, which can be an additional advantage of this LOPA technique.

The heat equation [29] was also solved using finite element model realized by Matlab to demonstrate that the heat induced by high excitation intensity of a 532 nm CW laser confines the crosslinking reaction in the local region where the temperature is higher than the PEB temperature. This resulted in fine and uniform structures, since only the material within the effective temperature region was properly polymerized. Temperature-depth dependence calculation shows that this technique allows the fabrication of uniform 3D sub-micro structures with large thickness. This is then evident by an experimental demonstration of fabrication of a uniform 3D woodpile structure without PEB step, with a period as small as 400 nm [28]. Compared to the commonly used TPA method, LOPA-based DLW with local PEB shows numerous advantages such as simple, low-cost setup and simplified fabrication process, while producing same high-quality structures.

4.2. Shrinkage effect

Shrinkage is a fundamental issue for photopolymerization in the photopolymer. It is difficult to avoid the non-uniformity when the conventional polymerized microstructures are attached to substrates. The origin of this effect for TPA polymerization has been investigated [30]. It was suggested that the origin of the shrinkage is the collapse of this material during the development stage owing to the polymer not being fully cross-linked when they are made at the irradiation power close to the photopolymerization threshold. At fabrication intensities slightly above the photopolymerization threshold, the photopolymerization yield is not

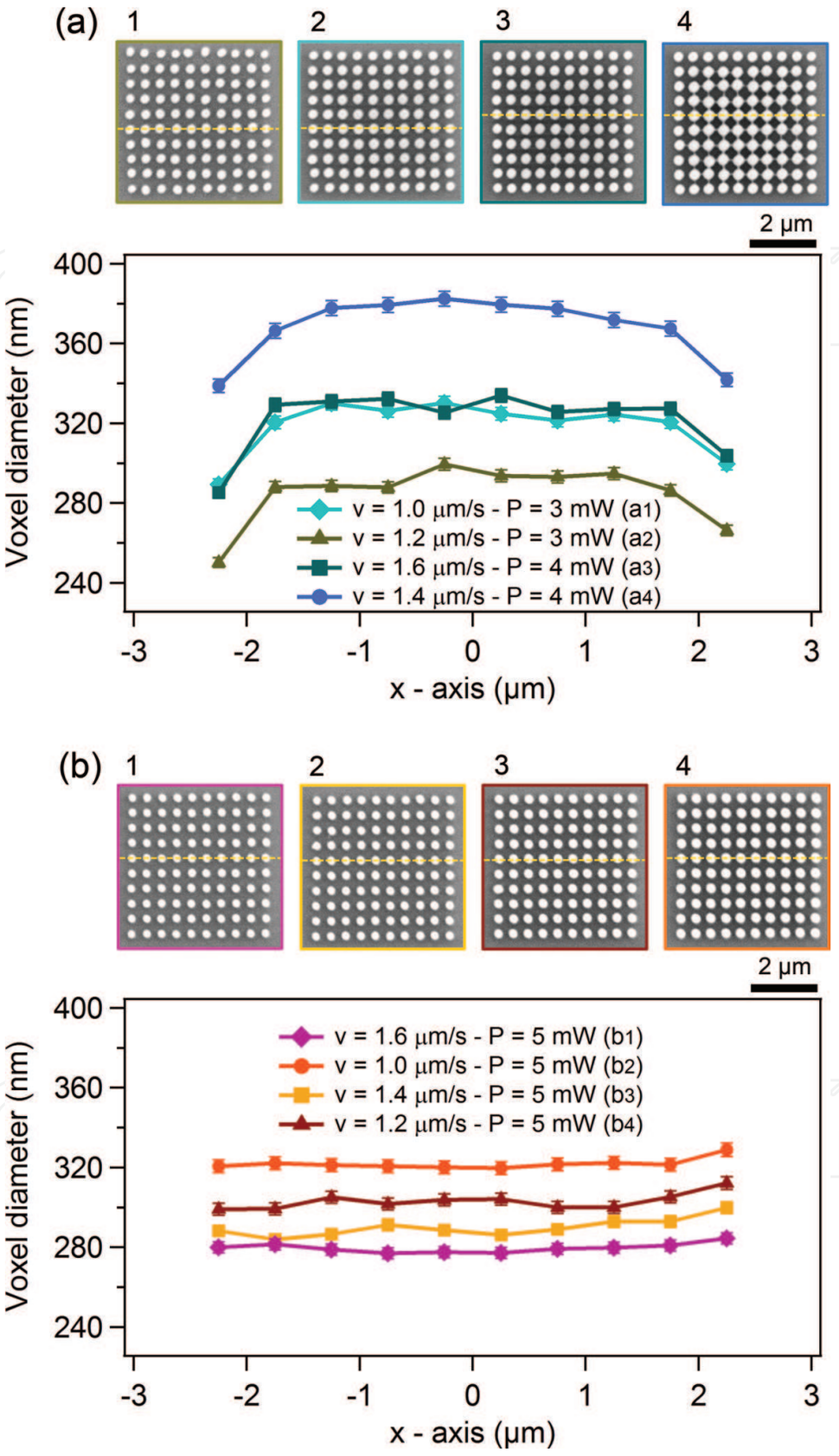

Figure 11. Comparison between structures fabricated with standard PEB (a) and local PEB (b) shows the advantage of "local PEB" in overcoming the accumulation effect. Left: SEM images of fabricated structures. Top: sizes of pillars indicated by the dashed line on SEM images plotted as a function of position. With standard PEB: the pillars are larger at center of pattern. With local PEB: pillars are very uniform. All structures are fabricated with a period of 500 nm.

100%, resulting in a sponge-like material after the development process. Hence, the structural shrinkage observed at average laser powers is the result of the collapse of this material at a molecular level [30]. However, it has also been confirmed that, although the sponge-like materials are formed during the development because of the non-full polymerization at low laser power, the shrinkage indeed occurs due to the capillary forces and the dramatic change of surface tension during the drying process [31].

For LOPA 3D fabrication, this shrinkage effect is also observed, with different levels of distortion for different exposure doses, i.e., the lower the exposure dose is the higher the shrinkage is. (**Figure 12a–d**) shows the shrinkage effect observed in 3D woodpile structures fabricated at different doses (P = 9 mW, writing speed v = 4, 3, 2, and 1 μm/s, from left to right, respectively). It can be clearly seen that the degree of shrinkage at different exposure doses is different, i.e., from left to right, the writing speed decreases (the dose increases), the shrinkage decreases. This result is also in agreement with previous report on the shrinkage in the case of TPA polymerization [30], which suggests that in both cases, the shrinkage effect might have a similar origin.

Non-uniform shrinkage might destroy the structural periodicity of a photonic crystal, resulting in the degradation of its optical quality. While shrinkage is an intrinsic problem, which cannot be avoided, non-uniform shrinkage problem can be positively resolved. Several approaches have been reported on how to overcome this non-uniform shrinkage, including pre-compensation for deformation [32], single [33] and multi-anchor supporting method [30, 34], or freestanding microstructures trapped in cages [35]. All the above methods are investigated for the TPA case. In this work, the multi-anchor supporting method was employed to reduce the deformation caused by the non-uniform shrinkage of 3D microstructures by LOPA DLW. To demonstrate this idea, instead of fabricating woodpile structures directly on glass substrate, four "legs" at four corners of structures were created in order to avoid the attachment of the structures to the glass substrate, which is the direct cause of the non-uniform

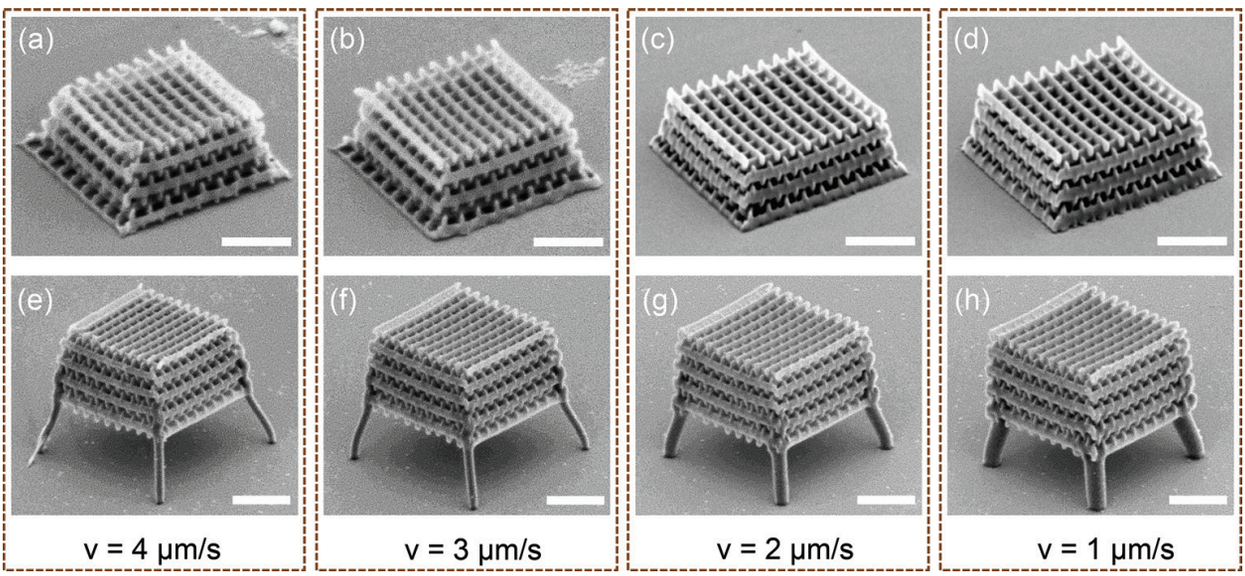

Figure 12. 3D woodpile structures (number of layers =16, rod spacing = 1.5 μm and layer spacing = 0.65 μm) fabricated without (a–d) and with "legs" (e–h), at laser power of 9 mW and different writing speeds: v = 4, 3, 2, and 1 μm/s, from left to right. Scale bars: 5 μm.

shrinkage. These anchors were designed and fabricated as rods of several hundred nanometers and did not affect the main structure. (**Figure 12e–h**) shows woodpile structures with anchors fabricated at different doses. It can be seen that at low dose, the non-uniform shrinkage still remains as shown in **Figure 12(e)**. However, when the dose is increased by a small amount, the distortion decreases and disappears. In this case, a laser power of 9 mW and a writing speed of 3 μm/s were sufficient for a considerable uniform structure. Compared to the non-anchored structures, the fabrication speed is reduced by three times to obtain a nearly deformation-free PC, which is remarkable especially for the fabrication of large structures. The shrinkage effect can also be exploited to produce PCs with small lattice constant.

To conclude, the multi-anchor supporting method was successfully applied to reduce the non-uniform deformation of 3D microstructure caused by attachment to the substrate. Since the support with four anchors allows uniform shrinkage of a polymeric microstructure by releasing it from the substrate, the fabricated microstructure shrinks isotropically. The combination of LOPA with local PEB and this supporting method is a promising way of producing small lattice constant photonic structures, which possess a photonic bandgap in the visible range.

5. Realization of magneto-photonic microstructures by LOPA-based DLW

LOPA-based DLW has been demonstrated to be not only applicable for SU8 but also other materials [36, 37], and be capable of fabricating structures incorporated with nanoparticles (NPs), such as plasmonic [38] or magnetic NPs [39]. In this section, as a proof of the versatility of LOPA DLW, the fabrication of 2D and 3D sub-microstructures from nanocomposite consisting of magnetite (Fe_3O_4) NPs and a commercial SU8 photoresist by employing LOPA DLW technique is presented [39]. The nanocomposite was synthesized by incorporating magnetic nanoparticles (MNPs) into SU8 matrix. Due to the magnetic force (mainly inter-particle interactions), MNPs tend to form large agglomerations, causing difficulties in achieving a homogeneous distribution of MNPs in polymer matrix. Hence, different concentrations of Fe_3O_4 MNPs and various types of SU8 with different viscosities have been investigated to obtain the best dispersion of MNPs in the polymer environment. Finally, the best compromise was achieved between SU8 2005, with moderate viscosity, and a MNP concentration of 2 wt%, which is low enough to achieve a homogeneous nanocomposite and high enough to give strong response to external magnetic field.

Arbitrary magnetic structures from magneto-polymer nanocomposite have been realized using LOPA DLW. **Figure 13(a)** shows an SEM image of an arbitrary 2D structure, the letter ”LPQM,” fabricated at the power of 15 mW with a writing speed of 3 μm/s. For this fabrication, a point matrix technique was used to shape the letter. The distance between pillars was set at 150 nm, which resulted in a continuous line due to the accumulation of exposure energy at the vicinity of each point. An SEM image of a 2D pillar array magneto-photonic structure, with a period of 1.5 μm is shown in **Figure 13(b)**. This structure was fabricated at

http://dx.doi.org/10.5772/intechopen.71318

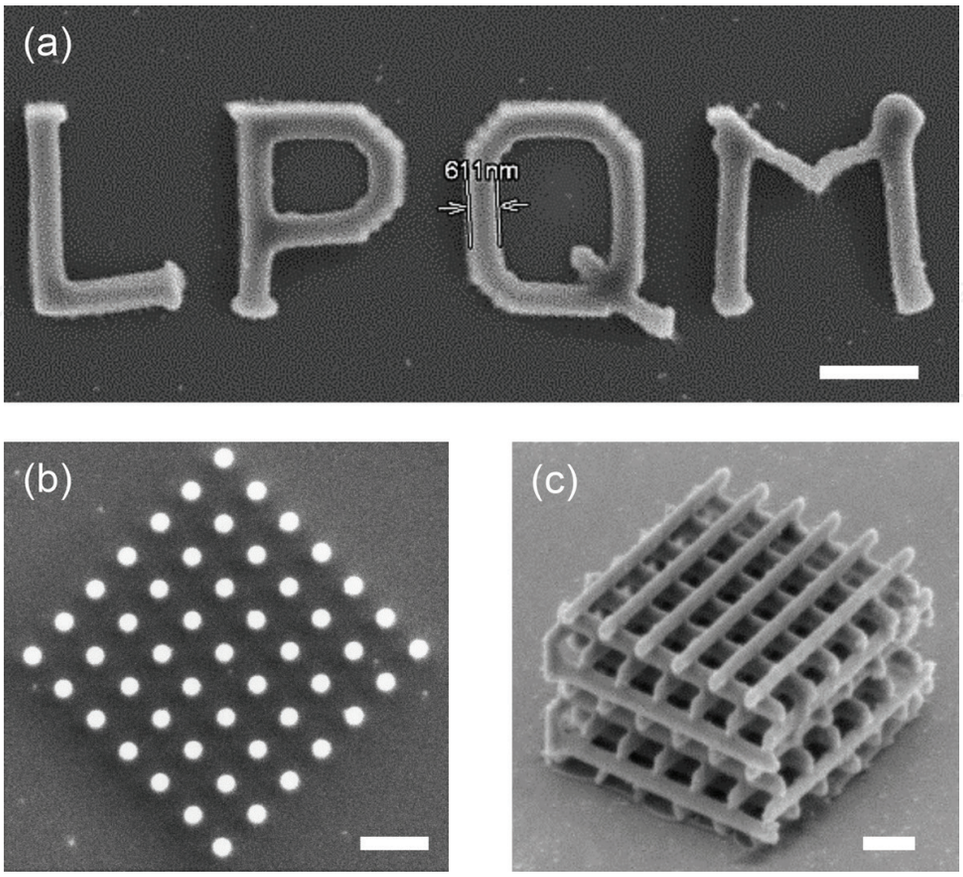

Figure 13. (a) SEM image of letter LPQM, fabricated at a laser power P = 15 mW, writing speed v = 3 μm/s. (b) SEM image of a 2D pillar array, fabricated at P = 12 mW, v = 2 μm/s. (c) SEM image of a 3D woodpile PC. Fabrication parameters: rod spacing = 2 μm; distance between layers = 1 μm; number of layers = 10; laser power P = 12 mW and scanning speed v = 2 μm/s. Scale bars: 2 μm.

a laser power of 12 mW and a writing speed of 2 μm/s. Similarly, various 3D structures have also been realized, with a laser power of about 12 mW. **Figure 13(c)** shows an SEM image of a woodpile structure, which consists of 10 alternating layers separated from each other by 1 μm. The rod spacing in x- and y-directions is 2 μm. These experimental results confirm that the LOPA-based DLW allows the fabrication of any magneto-photonic sub-micrometer structure or device on this magneto-polymer nanocomposite, which is very promising for a wide range of applications using magnetic microdevices and micro-robotic tools.

Indeed, magneto-photonic structures for remote actuation have attracted a great deal of attention recently [40]. With the aid of an external magnetic field, the displacement in three dimensions of magnetic structures can be controlled as desired. As shown previously, small magneto-photonic structures, which are adaptable to small targets, have been created. In order to prove the response of magnetic structures to a magnetic field, arrays of micro-pillars were fabricated as an example for demonstration [39]. To release the structures from the substrate, before coating the nanocomposite layer, an extra sacrificial layer of PMMA, which can be dissolved with acetone to release the structures into solution, was added. A magnetic field

(only 8 mT) generated by a permanent magnet was then applied to examine the magnetic field response of the magnetic micro-swimmers. The whole process from structural development to the movement toward higher gradient of the external magnetic field was observed via optical microscope, in which all of the micro-pillars quickly moved toward the magnetic tip, confirming the presence of Fe_3O_4 MNPs inside the structures and their strong response to the applied magnetic field. The magnetic structures responded strongly to the external magnetic field, opening many promising applications, such as tunable photonic structures based on magneto-optical effect and development of microrobotic tools for transport in biological systems.

6. Conclusions and prospects

In this chapter, a new technique based on an already-well-known mechanism, one-photon absorption (OPA) direct laser writing (DLW), for fabrication of low-cost, high-quality 3D PCs was introduced. This technique was demonstrated through both theory and experiment on the ultra-low absorption regime (LOPA) of photosensitive material. It was pointed out that DLW based on LOPA microscopy enables 3D fabrication in any kind of photoresist material with flexible defect engineering.

Some additional methods, such as dose compensation and local PEB, have been also proposed and applied to optimize the structures fabricated by LOPA DLW. In particular, by using the optically induced thermal effect, the fabrication of accumulation-free sub-micrometer and uniform polymeric 2D and 3D structures was realized. Also, the multi-anchor supporting method was employed to reduce the deformation caused by the non-uniform shrinkage of 3D polymeric microstructures.

As a proof of the versatility of the LOPA-based DLW technique, the capability to fabricate magneto-photonic microstructures using a SU8/Fe_3O_4 nanocomposite has been demonstrated. The fabricated micro-swimmers showed strong response to an applied external magnetic field, which emphasizes the importance of free-floating structures as a robotic technology for magnetic devices such as sensors, actuators, magnetic labeling, and drug targeting. 3D magneto-photonic structures have also been successfully fabricated, potentially aiding the development of magnetic nanodevices and micro-robotic tools for a wide range of applications.

Author details

Dam Thuy Trang Nguyen, Mai Trang Do, Qinggle Li, Quang Cong Tong, Thi Huong Au and Ngoc Diep Lai*

*Address all correspondence to: nlai@lpqm.ens-cachan.fr

Laboratoire de Photonique et Moléculaire, Ecole Normale Supérieure de Cachan, CentraleSupélec, CNRS, Université Paris-Saclay, Cachan, France

References

[1] Lin SY, Fleming JG, Hetherington DL, Smith BK, Biswas R, Ho KM, et al. A three-dimensional photonic crystal operating at infrared wavelengths. Nature. 1998;**394**(6690):251-253

[2] Cumpston BH, Ananthavel SP, Barlow S, Dyer DL, Ehrlich JE, Erskine LL, et al. Two-photon polymerization initiators for three-dimensional optical data storage and microfabrication. Nature. 1999;**398**:51-54

[3] Strickler JH, Webb WW. Three-dimensional data storage in refractive media by two-photon point excitation. Optics Letters. 1991;**16**:1780-1782

[4] Denk W, Strickler JH, Webb WW. Two-photon laser scanning fluorescence microscopy. Science. 1990;**248**:73-76

[5] Alkaisi MM, Blaikie RJ, McNab SJ, Cheung R, Cumming DRS. Sub-diffraction-limited patterning using evanescent near-field optical lithography. Applied Physics Letters. 1999;**75**(22):3560-3562

[6] Mata A, Fleischman A, Roy S. Fabrication of multi-layer SU-8 microstructures. Journal of Micromechanics and Microengineering. 2006;**16**:276-284

[7] Campbell M, Sharp DN, Harrison MT, Denning RG, Turberfield AJ. Fabrication of photonic crystals for the visible spectrum by holographic. Nature. 2000;**404**(6773):53-56

[8] Lai ND, Liang WP, Lin JH, Hsu CC, Lin CH. Fabrication of two- and three-dimensional periodic structures by multi-exposure of two-beam interference technique. Optics Express. 2005;**13**(23):9605-9611

[9] Lai ND, Zheng TS, Do DB, Lin JH, Hsu CC. Fabrication of desired three-dimensional structures by holographic assembly technique. Applied Physics A. 2010;**100**(1):171-175

[10] Seet KK, Mizeikis V, Juodkazis S, Misawa H. Three-dimensional horizontal circular spiral photonic crystals with stop gaps below 1 μm. Applied Physics Letters. 2006;**88**(22): 221101-221103

[11] Sun HB, Matsuo S, Misawa H. Three-dimensional photonic crystal structures achieved with two-photon absorption photopolymerization of resin. Applied Physics Letters. 1999;**74**(6):786-788

[12] Gissibl T, Thiele S, Herkommer A, Giessen H. Two-photon direct laser writing of ultracompact multi-lens objectives. Nature Photonics. 2016;**10**:554-560

[13] Straub M, Gu M. Near-infrared photonic crystals with higher-order bandgaps generated by two-photon photopolymerization. Optics Letters. 2002;**27**(20):1824-1826

[14] Rensch C, Hell S, Schickfus MV, Hunklinger S. Laser scanner for direct writing lithography. Applied Optics. 1989;**28**(17):3754-3758

[15] Bratton D, Yang D, Dai J, Ober CK. Recent progress in high resolution lithography. Polymers for Advanced Technologies. 2006;**17**:94-103

[16] Li Q, Do MT, Ledoux-Rak I, Lai ND. Concept for three-dimensional optical addressing by ultralow one-photon absorption method. Optics Letters. 2013;**38**(22):4640-4643

[17] Do MT, Nguyen TTN, Li Q, Benisty H, Ledoux-Rak I, Lai ND. Submicrometer 3D structures fabrication enabled by one-photon absorption direct laser writing. Optics Express. 2013;**21**(18):20964-20973

[18] Wolf E. Electromagnetic diffraction in optical systems I. An integral representation of the image field. Proceedings of the Royal Society A. 1959;**253**(1274):349-357

[19] Helseth LE. Focusing of atoms with strongly confined light potentials. Optics Communication. 2002;**212**(4-6):343-352

[20] Sun HB, Tanaka T, Kawata S. Three-dimensional focal spots related to two-photon excitation. Applied Physics Letters. 2002;**80**(20):3673-3675

[21] Lee CH, Chang TW, Lee KL, Lin JY, Wang J. Fabricating high-aspect-ratio sub-diffraction-limit structures on silicon with two-photon photopolymerization and reactive ion etching. Applied Physics A. 2004;**79**(8):2027-2031

[22] Do MT, Li Q, Ledoux-Rak I, and Lai ND. Optimization of LOPA-based direct laser writing technique for fabrication of submicrometric polymer two- and three-dimensional structures. Proc. SPIE 9127, Photonic Crystal Materials and Devices XI. 2014

[23] Matta JA, Outwater JO. The nature, origin and effects of internal stresses in reinforced plastic laminates. Polymer Engineering and Science. 1962;**2**(4):314-319

[24] Scott TF, Kloxin CJ, Forman DL, McLeod RR, Bowman CN. Principles of voxel refinement in optical direct write lithography. Journal of Materials Chemistry. 2011;**21**:14150-14155

[25] Chen KS, Lin IK, Ko FH. Fabrication of 3D polymer microstructures using electron beam lithography and nanoimprinting technologies. Journal of Micromechanics and Microengineering. 2005;**15**(10):1894-1903

[26] Correa DS, Boni LD, Otuka AJG, Tribuzi V, Mendonça CR. Two-photon polymerization fabrication of doped microstructures. In: De Souza Gomes A, editor. Polymerization. Rijeka: InTech; 2012

[27] Li L, Gattass RR, Gershgoren E, Hwang H, Fourkas JT. Achieving $\lambda/20$ resolution by one-color initiation and deactivation of polymerization. Science. 2009;**324**(5929):910-913

[28] Nguyen DTT, Tong QC, Ledoux-Rak I, Lai ND. One-step fabrication of submicrostructures by low one-photon absorption direct laser writing technique with local thermal effect. Journal of Applied Physics. 2016;**119**(1):013101-013106

[29] Carslaw HS, Jaeger JC. Conduction of Heat in Solids. 2nd ed. United Kingdom: Oxford University Press; 2000

[30] Ovsianikov A, Shizhou X, Farsari M, Vamvakaki M, Fotakis C, Chichkov BN. Shrinkage of microstructures produced by two-photon polymerization of Zr-based hybrid photosensitive materials. Optics Express. 2009;**17**(4):2143-2148

[31] Sun Q, Ueno K, Misawa H. In situ investigation of the shrinkage of photopolymerized micro/nanostructures: The effect of the drying process. Optics Letters. 2012;**37**(4):710-712

[32] Sun HB, Suwa T, Takada K, Zaccaria RP, Kim MS, Lee KS, et al. Shape precompensation in two-photon laser nanowriting of photonic lattices. Applied Physics Letters. 2004;**85**(17):3708-3710

[33] Maruo S, Hasegawa T, Yoshimura N. Single-anchor support and supercritical CO_2 drying enable high-precision microfabrication of three-dimensional structures. Optics Express. 2009;**17**(23):20945-20951

[34] Lim TW, Son Y, Yang SY, Pham TA, Kim DP, Yang BI, et al. Net shape manufacturing of three-dimensional SiCN ceramic microstructures using an isotropic shrinkage method by introducing shrinkage guiders. International Journal of Applied Ceramic Technology. 2008;**5**(3):258-264

[35] Sun Q, Juodkazis S, Murazawa N, Mizeikis V, Misawa H. Freestanding and movable photonic microstructures fabricated by photopolymerization with femtosecond laser pulses. Journal of Micromechanics and Microengineering. 2010;**20**(3):035004

[36] Mao F, Tong QC, Nguyen DTT, Huong AT, Odessey R, Saudrais F, et al. LOPA-based direct laser writing of multi-dimensional and multi-functional photonic submicrostructures. Proceedings of SPIE 10115, Advanced Fabrication Technologies for Micro/Nano Optics and Photonics X. 2017;1011509

[37] Tong QC, Luong MH, Remmel J, Do MT, Nguyen DTT, Lai ND. Rapid direct laser writing of desired plasmonic nanostructures. Optics Letters. 2017;**42**(12):2382-2385

[38] Do MT, Nguyen DTT, Ngo HM, Ledoux-Rak I, Lai ND. Controlled coupling of a single nanoparticle in polymeric microstructure by low one-photon absorption-based direct laser writing technique. Nanotechnology. 2015;**26**(10):105301

[39] TH A, Trinh DT, Tong QC, Do DB, Nguyen DP, Phan MH. Direct laser writing of magneto-photonic sub-microstructures for prospective applications in biomedical engineering. Nanomaterials. 2017;**7**(5):105

[40] Markides H, Rotherham M, El Haj AJ. Biocompatibility and toxicity of magnetic nanoparticles in regenerative medicine, biocompatibility and toxicity of magnetic nanoparticles in regenerative medicine. Journal of Nanomaterials. 2012;**2012**:614094

IntechOpen